Chapter 8 / Failure

8.5W Principles of Fracture Mechanics (Detailed Version)

Brittle fracture of normally ductile materials, such as that shown in the chapter-opening photograph of this chapter in the text, has demonstrated the need for a better understanding of the mechanisms of fracture. Extensive research endeavors over the past several decades have led to the evolution of the field of **fracture mechanics.** This subject allows quantification of the relationships between material properties, stress level, the presence of crack-producing flaws, and crack propagation mechanisms. Design engineers are now better equipped to anticipate, and thus prevent, structural failures. The present discussion centers on some of the fundamental principles of the mechanics of fracture.

STRESS CONCENTRATION

The fracture strength of a solid material is a function of the cohesive forces that exist between atoms. On this basis, the theoretical cohesive strength of a brittle elastic solid has been estimated to be approximately $E/10$, where E is the modulus of elasticity. The experimental fracture strengths of most engineering materials normally lie between 10 and 1000 times below this theoretical value. In the 1920s, A. A. Griffith proposed that this discrepancy between theoretical cohesive strength and observed fracture strength could be explained by the presence of very small, microscopic flaws or cracks that always exist under normal conditions at the surface and within the interior of a body of material. These flaws are a detriment to the fracture strength because an applied stress may be amplified or concentrated at the tip, with the magnitude of this amplification depending on crack orientation and geometry. This phenomenon is demonstrated in Figure 8.1W, a stress profile across a cross section containing an internal crack. As indicated by this profile, the magnitude of this localized stress diminishes with distance away from the crack tip. At positions far removed, the stress is equal to the nominal stress σ_0, or the applied load divided by the specimen cross-sectional area (perpendicular to this load). Due to their ability to amplify an applied stress in their locale, these flaws are sometimes called **stress raisers.**

If it is assumed that a crack is similar to an elliptical hole through a plate and is oriented perpendicular to the applied stress, the maximum stress, σ_m, at the crack tip is equal to

$$\sigma_m = \sigma_0\left[1 + 2\left(\frac{a}{\rho_t}\right)^{1/2}\right] \tag{8.1W}$$

where σ_0 is the magnitude of the nominal applied tensile stress, ρ_t is the radius of curvature of the crack tip (Figure 8.1aW), and a represents the length of a surface

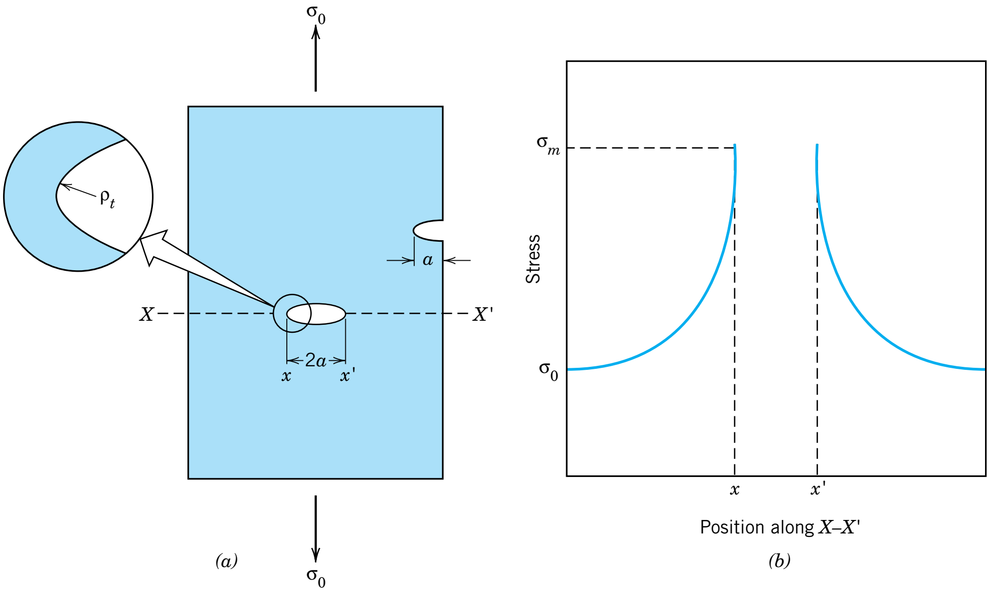

Figure 8.1W (*a*) The geometry of surface and internal cracks. (*b*) Schematic stress profile along the line X–X' in (*a*), demonstrating stress amplification at crack tip positions.

crack, or half of the length of an internal crack. For a relatively long microcrack that has a small tip radius of curvature, the factor $(a/\rho_t)^{1/2}$ may be very large (certainly much greater than unity); under these circumstances Equation 8.1W takes the form

$$\sigma_m = 2\sigma_0\left(\frac{a}{\rho_t}\right)^{1/2} \tag{8.2W}$$

Furthermore, σ_m will be many times the value of σ_0.

Sometimes the ratio σ_m/σ_0 is denoted as the *stress concentration factor* K_t:

$$K_t = \frac{\sigma_m}{\sigma_0} = 2\left(\frac{a}{\rho_t}\right)^{1/2} \tag{8.3W}$$

which is simply a measure of the degree to which an external stress is amplified at the tip of a crack.

Note that stress amplification is not restricted to these microscopic defects; it may occur at macroscopic internal discontinuities (e.g., voids), at sharp corners, and at notches in large structures. Figure 8.2W shows theoretical stress concentration factor curves for several simple and common macroscopic discontinuities.

Furthermore, the effect of a stress raiser is more significant in brittle than in ductile materials. For a ductile material, plastic deformation ensues when the maximum stress exceeds the yield strength. This leads to a more uniform distribution of stress in the vicinity of the stress raiser and to the development of a maximum stress concentration factor less than the theoretical value. Such yielding and stress redistribution do not occur to any appreciable extent around flaws

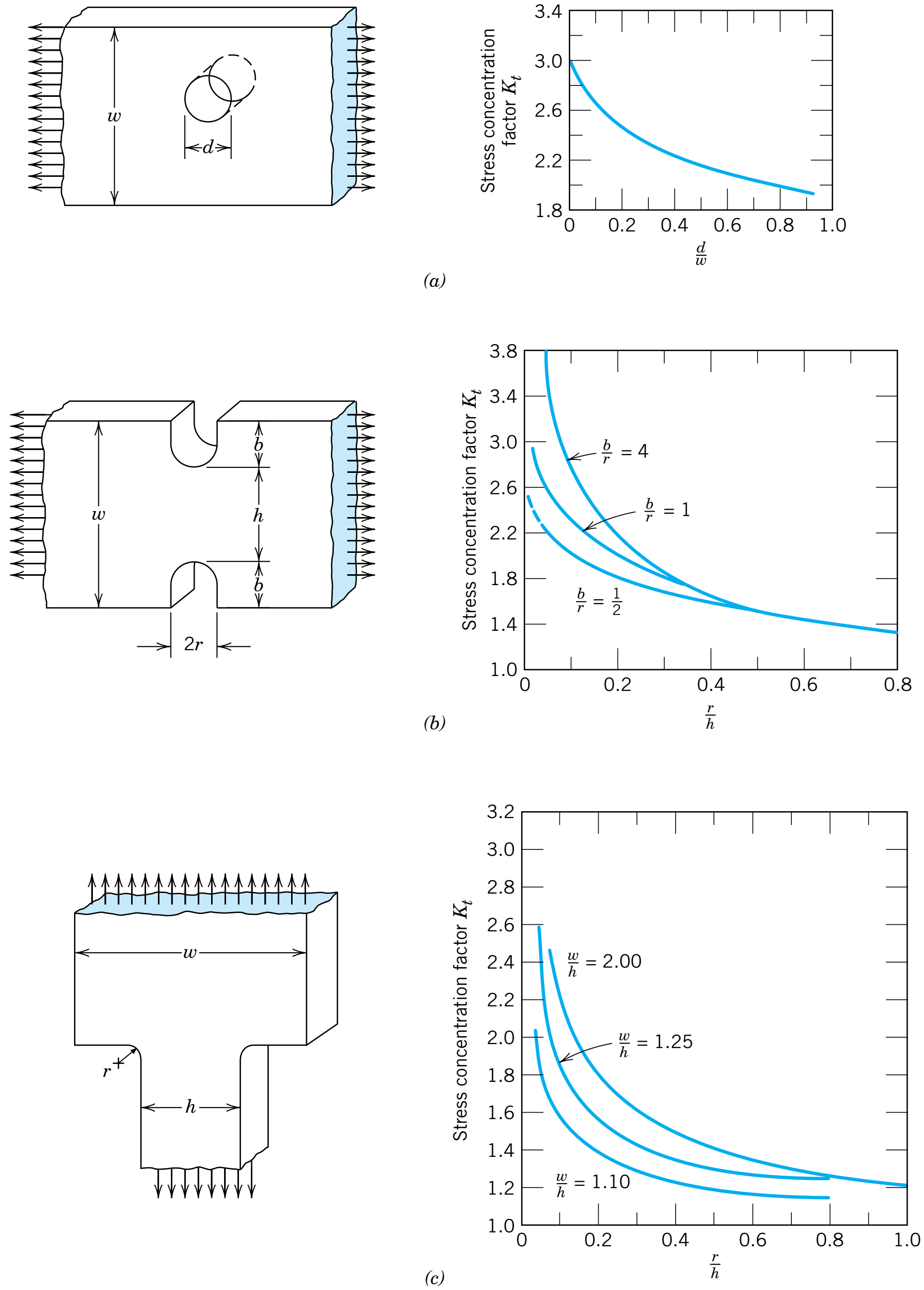

FIGURE 8.2W Theoretical stress concentration factor curves for three simple geometrical shapes. (From G. H. Neugebauer, *Prod. Eng.* NY), Vol. 14, pp. 82–87, 1943.)

and discontinuities in brittle materials; therefore, essentially the theoretical stress concentration will result.

Griffith then went on to propose that all brittle materials contain a population of small cracks and flaws that have a variety of sizes, geometries, and orientations. Fracture will result when, upon application of a tensile stress, the theoretical cohesive strength of the material is exceeded at the tip of one of these flaws. This leads to the formation of a crack that then rapidly propagates. If no flaws were present, the fracture strength would be equal to the cohesive strength of the material. Very small and virtually defect-free metallic and ceramic whiskers have been grown with fracture strengths that approach their theoretical values.

GRIFFITH THEORY OF BRITTLE FRACTURE

During the propagation of a crack, there is a release of what is termed the *elastic strain energy,* some of the energy that is stored in the material as it is elastically deformed. Furthermore, during the crack extension process, new free surfaces are created at the faces of a crack, which give rise to an increase in surface energy of the system. Griffith developed a criterion for crack propagation of an elliptical crack (Figure 8.1*a*W) by performing an energy balance using these two energies. He demonstrated that the critical stress σ_c required for crack propagation in a brittle material is described by

$$\sigma_c = \left(\frac{2E\gamma_s}{\pi a}\right)^{1/2} \tag{8.4W}$$

where

E = modulus of elasticity

γ_s = specific surface energy

a = one half the length of an internal crack

Worth noting is that this expression does not involve the crack tip radius ρ_t, as does the stress concentration equation (Equation 8.1W); however, it is assumed that the radius is sufficiently sharp (on the order of the interatomic spacing) so as to raise the local stress at the tip above the cohesive strength of the material.

The previous development applies only to completely brittle materials, for which there is no plastic deformation. Most metals and many polymers do experience some plastic deformation during fracture; thus, crack extension involves more than producing just an increase in the surface energy. This complication may be accommodated by replacing γ_s in Equation 8.4W by $\gamma_s + \gamma_p$, where γ_p represents a plastic deformation energy associated with crack extension. Thus,

$$\sigma_c = \left[\frac{2E(\gamma_s + \gamma_p)}{\pi a}\right]^{1/2} \tag{8.5W}$$

For highly ductile materials, it may be the case that $\gamma_p \gg \gamma_s$ such that

$$\sigma_c = \left(\frac{2E\gamma_p}{\pi a}\right)^{1/2} \tag{8.6W}$$

In the 1950s, G. R. Irwin chose to incorporate both γ_s and γ_p into a single term, $\mathcal{G}_c$, as

$$\mathcal{G}_c = 2(\gamma_s + \gamma_p) \tag{8.7W}$$

$\mathcal{G}_c$ is known as the *critical strain energy release rate.* Incorporation of Equation 8.7W into Equation 8.5W after some rearrangement leads to another expression for the

Griffith cracking criterion as

$$\mathcal{G}_c = \frac{\pi\sigma^2 a}{E} \tag{8.8W}$$

Thus, crack extension occurs when $\pi\sigma^2 a/E$ exceeds the value of $\mathcal{G}_c$ for the particular material under consideration.

Example Problem 8.1W

A relatively large plate of a glass is subjected to a tensile stress of 40 MPa. If the specific surface energy and modulus of elasticity for this glass are 0.3 J/m^2 and 69 GPa, respectively, determine the maximum length of a surface flaw that is possible without fracture.

Solution

To solve this problem it is necessary to employ Equation 8.4W. Rearrangement of this expression such that a is the dependent variable, and realizing that $\sigma = 40$ MPa, $\gamma_s = 0.3$ J/m^2, and $E = 69$ GPa, leads to

$$\begin{aligned} a &= \frac{2E\gamma_s}{\pi\sigma^2} \\ &= \frac{(2)(69 \times 10^9 \text{ N/m}^2)(0.3 \text{ N/m})}{\pi(40 \times 10^6 \text{ N/m}^2)^2} \\ &= 8.2 \times 10^{-6} \text{ m} = 0.0082 \text{ mm} = 8.2\ \mu\text{m} \end{aligned}$$

STRESS ANALYSIS OF CRACKS

As we continue to explore the development of fracture mechanics, it is worthwhile to examine the stress distributions in the vicinity of the tip of an advancing crack. There are three fundamental ways, or modes, by which a load can operate on a crack, and each will affect a different crack surface displacement; these are illustrated in Figure 8.3W. Mode I is an opening (or tensile) mode, whereas modes II and III are sliding and tearing modes, respectively. Mode I is encountered most frequently, and only it will be treated in the ensuing discussion on fracture mechanics.

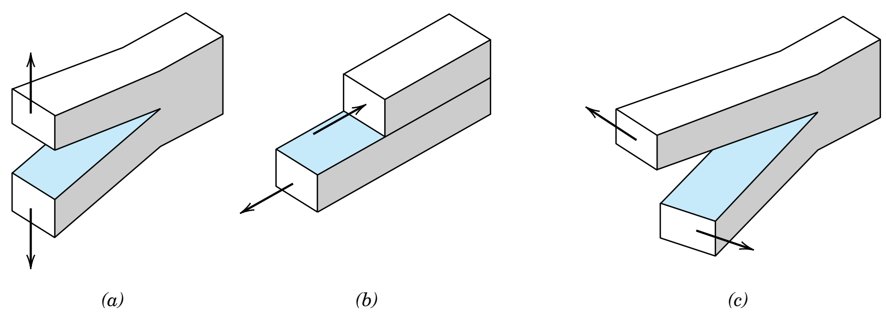

Figure 8.3W The three modes of crack surface displacement. (*a*) Mode I, opening or tensile mode; (*b*) mode II, sliding mode; and (*c*) mode III, tearing mode.

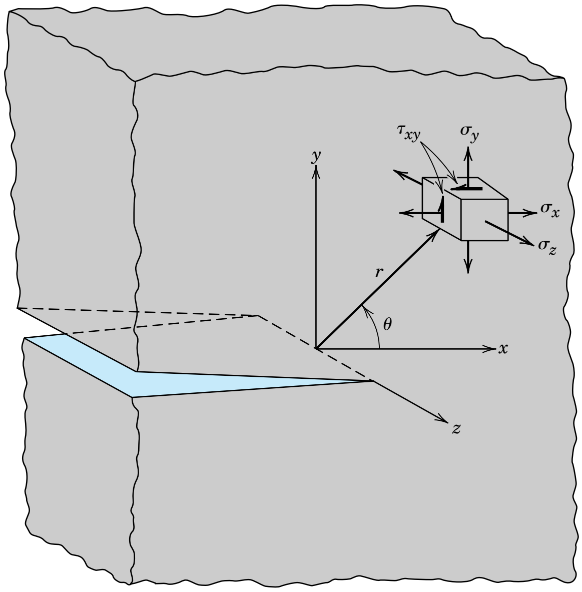

FIGURE 8.4W The stresses acting in front of a crack that is loaded in a tensile mode I configuration.

For this mode I configuration, the stresses acting on an element of material are shown in Figure 8.4W. Using elastic theory principles and the notation indicated, tensile (σ_x and σ_y)[1] and shear (τ_{xy}) stresses are functions of both radial distance r and the angle θ as follows:[2]

$$\boxed{\sigma_x = \frac{K}{\sqrt{2\pi r}} f_x(\theta)} \tag{8.9aW}$$

$$\boxed{\sigma_y = \frac{K}{\sqrt{2\pi r}} f_y(\theta)} \tag{8.9bW}$$

$$\boxed{\tau_{xy} = \frac{K}{\sqrt{2\pi r}} f_{xy}(\theta)} \tag{8.9cW}$$

If the plate is thin relative to the dimensions of the crack, then $\sigma_z = 0$, or a condition of *plane stress* is said to exist. At the other extreme (a relatively thick plate), $\sigma_z = \nu(\sigma_x + \sigma_y)$, and the state is referred to as **plane strain** (since $\epsilon_z = 0$); ν in this expression is Poisson's ratio.

---

[1] This σ_y denotes a tensile stress parallel to the y-direction, and should not be confused with the yield strength (Section 6.6), which uses the same symbol.

[2] The $f(\theta)$ functions are as follows:

$$f_x(\theta) = \cos\frac{\theta}{2}\left(1 - \sin\frac{\theta}{2}\sin\frac{3\theta}{2}\right)$$

$$f_y(\theta) = \cos\frac{\theta}{2}\left(1 + \sin\frac{\theta}{2}\sin\frac{3\theta}{2}\right)$$

$$f_{xy}(\theta) = \sin\frac{\theta}{2}\cos\frac{\theta}{2}\cos\frac{3\theta}{2}$$

In Equations 8.9W, the parameter K is termed the **stress intensity factor;** its use provides for a convenient specification of the stress distribution around a flaw. Note that this stress intensity factor and the stress concentration factor K_t in Equation 8.3W, although similar, are not equivalent.

The stress intensity factor is related to the applied stress and the crack length by the following equation:

$$K = Y\sigma\sqrt{\pi a} \tag{8.10W}$$

Here Y is a dimensionless parameter or function that depends on both the crack and specimen sizes and geometries, as well as the manner of load application. More will be said about Y in the discussion that follows. Moreover, note that K has the unusual units of MPa$\sqrt{\text{m}}$ (psi$\sqrt{\text{in.}}$ [alternatively ksi$\sqrt{\text{in.}}$]).

FRACTURE TOUGHNESS

In the previous discussion, a criterion was developed for the crack propagation in a brittle material containing a flaw; fracture occurs when the applied stress level exceeds some critical value σ_c (Equation 8.4W). Similarly, since the stresses in the vicinity of a crack tip can be defined in terms of the stress intensity factor, a critical value of K exists that may be used to specify the conditions for brittle fracture; this critical value is termed the **fracture toughness** K_c, and, from Equation 8.10W, is defined by

$$K_c = Y(a/W)\sigma_c\sqrt{\pi a} \tag{8.11W}$$

Here σ_c again is the critical stress for crack propagation, and we now represent Y as a function of both crack length (a) and component width (W)—that is, as $Y(a/W)$.

Relative to this $Y(a/W)$ function, as the a/W ratio approaches zero (i.e., for very wide planes and short cracks), $Y(a/W)$ approaches a value of unity. For example, for a plate of infinite width having a through-thickness crack, Figure 8.5*a*W, $Y(a/W) = 1.0$; for a plate of semi-infinite width containing an edge crack of length a (Figure 8.5*b*W), $Y(a/W) \cong 1.1$. Mathematical expressions for $Y(a/W)$ (often relatively

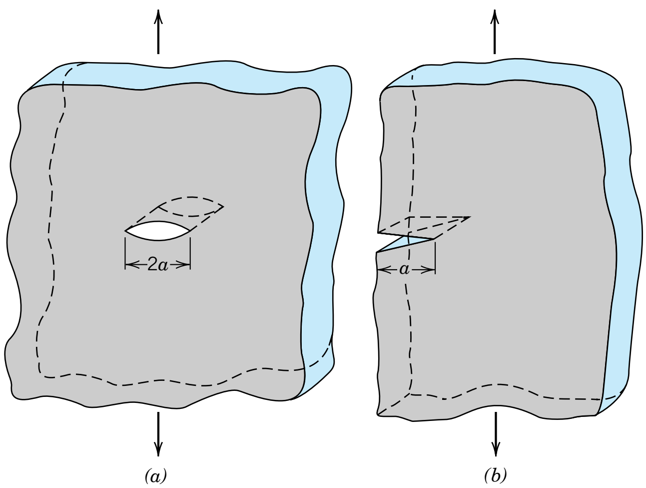

FIGURE 8.5W Schematic representations of (*a*) an interior crack in a plate of infinite width, and (*b*) an edge crack in a plate of semi-infinite width.

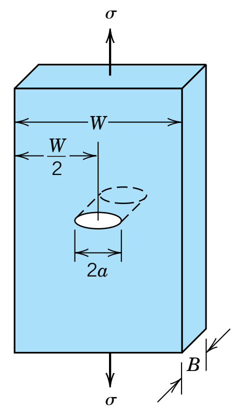

Figure 8.6W Schematic representation of a flat plate of finite width having a through-thickness center crack.

complex) in terms of a/W are required for components of finite dimensions. For example, for a center-cracked (through-thickness) plate of width W (Figure 8.6W)

$$Y(a/W) = \left(\frac{W}{\pi a}\tan\frac{\pi a}{W}\right)^{1/2} \tag{8.12W}$$

Here the $\pi a/W$ argument for the tangent is expressed in radians, not degrees. It is often the case for some specific component-crack configuration that $Y(a/W)$ is plotted versus a/W (or some variation of a/W). Several of these plots are shown in Figures 8.7*a*W, *b*W, and *c*W; included in the figures are equations that are used to determine K_cs.

By definition, fracture toughness is a property that is the measure of a material's resistance to brittle fracture when a crack is present. Its units are the same as for the stress intensity factor (i.e., MPa$\sqrt{\text{m}}$ or psi$\sqrt{\text{in.}}$).

For relatively thin specimens, the value of K_c will depend on and decrease with increasing specimen thickness B, as indicated in Figure 8.8W. Eventually, K_c becomes independent of B, at which time the condition of plane strain is said to exist.[3] The constant K_c value for thicker specimens is known as the **plane strain fracture toughness** K_{Ic}, which is also defined by[4]

$$K_{Ic} = Y\sigma\sqrt{\pi a} \tag{8.13W}$$

It is the fracture toughness normally cited since its value is always less than K_c. The I subscript for K_{Ic} denotes that this critical value of K is for mode I crack displacement, as illustrated in Figure 8.3*a*W. Brittle materials, for which appreciable plastic deformation is not possible in front of an advancing crack, have low K_{Ic} values and are vulnerable to catastrophic failure. On the other hand, K_{Ic}

---

[3] Experimentally, it has been verified that for plane strain conditions

$$B \geq 2.5\left(\frac{K_{Ic}}{\sigma_y}\right)^2 \tag{8.14W}$$

where σ_y is the 0.002 strain offset yield strength of the material.

[4] In the ensuing discussion we will use Y to designate $Y(a/W)$, in order to simplify the form of the equations.

FIGURE 8.7W *Y* calibration curves for three simple crack-plate geometries. (Copyright ASTM. Reprinted with permission.)

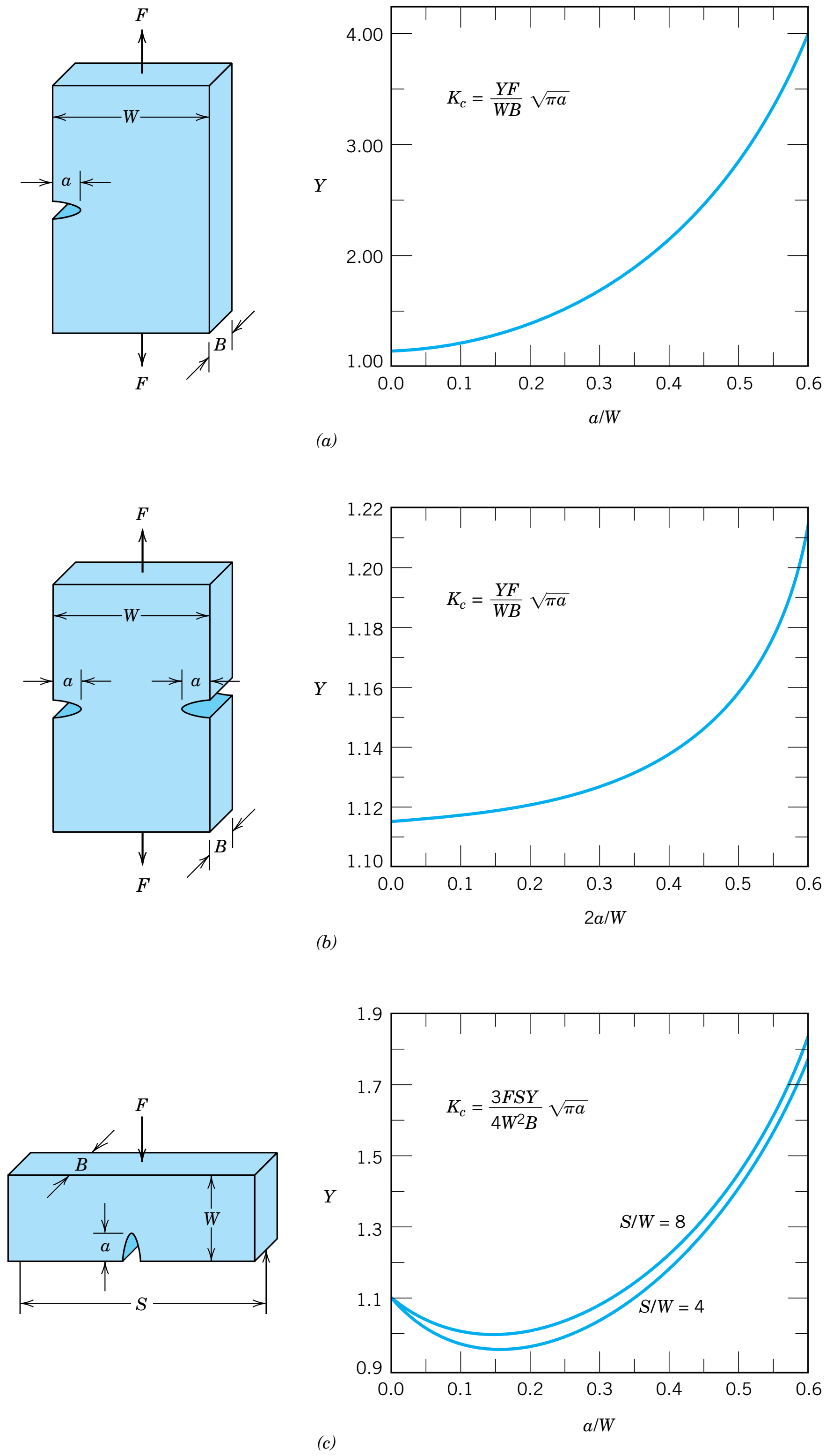

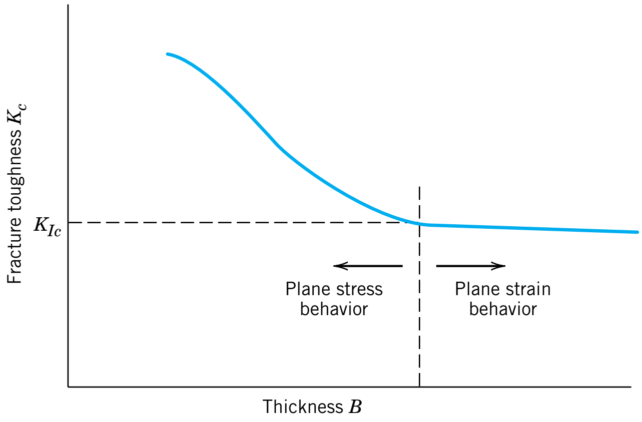

FIGURE 8.8W Schematic representation showing the effect of plate thickness on fracture toughness.

values are relatively large for ductile materials. Fracture mechanics is especially useful in predicting catastrophic failure in materials having intermediate ductilities. Plane strain fracture toughness values for a number of different materials are presented in Table 8.1W; a more extensive list of K_{Ic} values is contained in Table B.5, Appendix B.

Table 8.1W Room-Temperature Yield Strength and Plane Strain Fracture Toughness Data for Selected Engineering Materials

	Yield Strength		K_{Ic}	
Material	*MPa*	*ksi*	$MPa\sqrt{m}$	$ksi\sqrt{in.}$
Metals				
Aluminum alloy[a] (7075-T651)	495	72	24	22
Aluminum alloy[a] (2024-T3)	345	50	44	40
Titanium alloy[a] (Ti-6Al-4V)	910	132	55	50
Alloy steel[a] (4340 tempered @ 260°C)	1640	238	50.0	45.8
Alloy steel[a] (4340 tempered @ 425°C)	1420	206	87.4	80.0
Ceramics				
Concrete	—	—	0.2–1.4	0.18–1.27
Soda–lime glass	—	—	0.7–0.8	0.64–0.73
Aluminum oxide	—	—	2.7–5.0	2.5–4.6
Polymers				
Polystyrene (PS)	—	—	0.7–1.1	0.64–1.0
Polymethyl methacrylate (PMMA)	53.8–73.1	7.8–10.6	0.7–1.6	0.64–1.5
Polycarbonate (PC)	62.1	9.0	2.2	2.0

[a] **Source:** Reprinted with permission, *Advanced Materials and Processes,* ASM International, © 1990.

The stress intensity factor K in Equations 8.9W and the plane strain fracture toughness K_{Ic} are related to one another in the same sense as are stress and yield strength. A material may be subjected to many values of stress; however, there is a specific stress level at which the material plastically deforms—that is, the yield strength. Likewise, a variety of K's are possible, whereas K_{Ic} is unique for a particular material, and indicates the conditions of flaw size and stress necessary for brittle fracture.

Several different testing techniques are used to measure K_{Ic}.[5] Virtually any specimen size and shape consistent with mode I crack displacement may be utilized, and accurate values will be realized provided that the Y scale parameter in Equation 8.13W has been properly determined.

The plane strain fracture toughness K_{Ic} is a fundamental material property that depends on many factors, the most influential of which are temperature, strain rate, and microstructure. The magnitude of K_{Ic} diminishes with increasing strain rate and decreasing temperature. Furthermore, an enhancement in yield strength wrought by solid solution or dispersion additions or by strain hardening generally produces a corresponding decrease in K_{Ic}. Furthermore, K_{Ic} normally increases with reduction in grain size as composition and other microstructural variables are maintained constant. Yield strengths are included for some of the materials listed in Table 8.1W.

DESIGN USING FRACTURE MECHANICS

According to Equations 8.11W and 8.13W, three variables must be considered relative to the possibility for fracture of some structural component—namely, the fracture toughness (K_c) or plane strain fracture toughness (K_{Ic}), the imposed stress (σ), and the flaw size (a), assuming, of course, that Y has been determined. When designing a component, it is first important to decide which of these variables are constrained by the application and which are subject to design control. For example, material selection (and hence K_c or K_{Ic}) is often dictated by factors such as density (for lightweight applications) or the corrosion characteristics of the environment. Or, the allowable flaw size is either measured or specified by the limitations of available flaw detection techniques. It is important to realize, however, that once any combination of two of the above parameters is prescribed, the third becomes fixed (Equations 8.11W and 8.13W). For example, assume that K_{Ic} and the magnitude of a are specified by application constraints; therefore, the design (or critical) stress σ_c must be

$$\sigma_c \leq \frac{K_{Ic}}{Y\sqrt{\pi a}} \tag{8.15W}$$

On the other hand, if stress level and plane strain fracture toughness are fixed by the design situation, then the maximum allowable flaw size a_c is

$$a_c = \frac{1}{\pi}\left(\frac{K_{Ic}}{\sigma Y}\right)^2 \tag{8.16W}$$

---

[5] See for example ASTM Standard E 399, "Standard Test Method for Plane Strain Fracture Toughness of Metallic Materials."

A number of nondestructive test (NDT) techniques have been developed that permit detection and measurement of both internal and surface flaws. Such NDT methods are used to avoid the occurrence of catastrophic failure by examining structural components for defects and flaws that have dimensions approaching the critical size.

EXAMPLE PROBLEM 8.2W

A structural component in the form of a very wide plate, as shown in Figure 8.5*a*W, is to be fabricated from a 4340 steel. Two sheets of this alloy, each having a different heat treatment and thus different mechanical properties, are available. One, denoted material A, has a yield strength of 860 MPa (125,000 psi) and a plane strain fracture toughness of 98.9 MPa$\sqrt{\text{m}}$ (90 ksi$\sqrt{\text{in.}}$). For the other, material Z, σ_y and K_{Ic} values are 1515 MPa (220,000 psi) and 60.4 MPa$\sqrt{\text{m}}$ (55 ksi$\sqrt{\text{in.}}$), respectively.

(a) For each alloy, determine whether or not plane strain conditions prevail if the plate is 10 mm (0.39 in.) thick.

(b) It is not possible to detect flaw sizes less than 3 mm, which is the resolution limit of the flaw detection apparatus. If the plate thickness is sufficient such that the K_{Ic} value may be used, determine whether or not a critical flaw is subject to detection. Assume that the design stress level is one-half of the yield strength; also, for this configuration, the value of Y is 1.0.

Solution

(a) Plane strain is established by Equation 8.14W. For material A,

$$B = 2.5\left(\frac{K_{Ic}}{\sigma_y}\right)^2 = 2.5\left(\frac{98.9\ \text{MPa}\sqrt{\text{m}}}{860\ \text{MPa}}\right)^2$$
$$= 0.033\ \text{m} = 33\ \text{mm}\ (1.30\ \text{in.})$$

Thus, plane strain conditions *do not* hold for material A because this value of B is greater than 10 mm, the actual plate thickness; the situation is one of plane stress and must be treated as such.

For material Z,

$$B = 2.5\left(\frac{60.4\ \text{MPa}\sqrt{\text{m}}}{1515\ \text{MPa}}\right)^2 = 0.004\ \text{m} = 4.0\ \text{mm}\ (0.16\ \text{in.})$$

which is less than the actual plate thickness, and therefore the situation is one of plane strain.

(b) We need only determine the critical flaw size for material Z because the situation for material A is not plane strain, and K_{Ic} may not be used. Employing Equation 8.16W and taking σ to be $\sigma_y/2$,

$$a_c = \frac{1}{\pi}\left(\frac{60.4\ \text{MPa}\sqrt{\text{m}}}{(1)(1515/2)\,\text{MPa}}\right)^2$$
$$= 0.002\ \text{m} = 2.0\ \text{mm}\ (0.079\ \text{in.})$$

Therefore, the critical flaw size for material Z is not subject to detection since it is less than 3 mm.

Design Example 8.1W

Consider the thin-walled spherical tank of radius r and thickness t (Figure 8.9W) that may be used as a pressure vessel.

(a) One design of such a tank calls for yielding of the wall material prior to failure as a result of the formation of a crack of critical size and its subsequent rapid propagation. Thus, plastic distortion of the wall may be observed and the pressure within the tank released before the occurrence of catastrophic failure. Consequently, materials having large critical crack lengths are desired. On the basis of this criterion, rank the metal alloys listed in Table B.5, Appendix B, as to critical crack size, from longest to shortest.

(b) An alternative design that is also often utilized with pressure vessels is termed *leak-before-break*. Using principles of fracture mechanics, allowance is made for the growth of a crack through the thickness of the vessel wall prior to the occurrence of rapid crack propagation (Figure 8.9W). Thus, the crack will completely penetrate the wall without catastrophic failure, allowing for its detection by the leaking of pressurized fluid. With this criterion the critical crack length a_c (i.e., one-half of the total internal crack length) is taken to be equal to the pressure vessel thickness t. Allowance for $a_c = t$ instead of $a_c = t/2$ assures that fluid leakage will occur prior to the buildup of dangerously high pressures. Using this criterion, rank the metal alloys in Table B.5, Appendix B as to the maximum allowable pressure.

For this spherical pressure vessel, the circumferential wall stress σ is a function of the pressure p in the vessel and the radius r and wall thickness t according to

$$\sigma = \frac{pr}{2t} \tag{8.17W}$$

For both parts (a) and (b) assume a condition of plane strain.

Solution

(a) For the first design criterion, it is desired that the circumferential wall stress be less than the yield strength of the material. Substitution of σ_y for σ in Equation 8.13W,

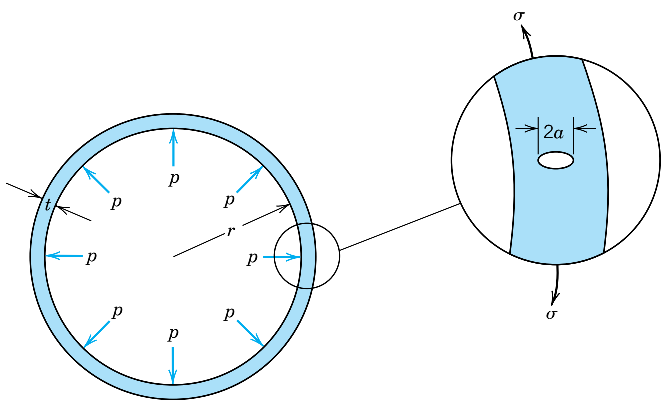

Figure 8.9W Schematic diagram showing the cross section of a spherical tank that is subjected to an internal pressure p, and that has a radial crack of length $2a$ in its wall.

and incorporation of a factor of safety N leads to

$$K_{Ic} = Y\left(\frac{\sigma_y}{N}\right)\sqrt{\pi a_c} \tag{8.18W}$$

where a_c is the critical crack length. Solving for a_c yields the following expression:

$$a_c = \frac{N^2}{Y^2\pi}\left(\frac{K_{Ic}}{\sigma_y}\right)^2 \tag{8.19W}$$

Therefore, the critical crack length is proportional to the square of the K_{Ic}–σ_y ratio, which is the basis for the ranking of the metal alloys in Table B.5. The ranking is provided in Table 8.2W, where it may be seen that the medium carbon (1040) steel with the largest ratio has the longest critical crack length and, therefore, is the most desirable material on the basis of this criterion.

(b) As stated previously, the leak-before-break criterion is just met when one-half of the internal crack length is equal to the thickness of the pressure vessel—that is, when $a = t$. Substitution of $a = t$ into Equation 8.13W gives

$$K_{Ic} = Y\sigma\sqrt{\pi t} \tag{8.20W}$$

From Equation 8.17W,

$$t = \frac{pr}{2\sigma} \tag{8.21W}$$

The stress is replaced by the yield strength, inasmuch as the tank should be designed to contain the pressure without yielding; furthermore, substitution of

Table 8.2W Ranking of Several Metal Alloys Relative to Critical Crack Length (Yielding Criterion) for a Thin-Walled Spherical Pressure Vessel

Material	$\left(\frac{K_{Ic}}{\sigma_y}\right)^2$ (*mm*)
Medium carbon (1040) steel	43.1
AZ31B magnesium	19.6
2024 aluminum (T3)	16.3
Ti-5Al-2.5Sn titanium	6.6
4140 steel (tempered @ 482°C)	5.3
4340 steel (tempered @ 425°C)	3.8
Ti-6Al-4V titanium	3.7
17-7PH steel	3.4
7075 aluminum (T651)	2.4
4140 steel (tempered @ 370°C)	1.6
4340 steel (tempered @ 260°C)	0.93

Table 8.3W **Ranking of Several Metal Alloys Relative to Maximum Allowable Pressure (Leak-Before-Break Criterion) for a Thin-Walled Spherical Pressure Vessel**

Material	$\frac{K_{Ic}^2}{\sigma_y}$ *(MPa-m)*
Medium carbon (1040) steel	11.2
4140 steel (tempered @ 482°C)	6.1
Ti-5Al-2.5Sn titanium	5.8
2024 aluminum (T3)	5.6
4340 steel (tempered @ 425°C)	5.4
17-7PH steel	4.4
AZ31B magnesium	3.9
Ti-6Al-4V titanium	3.3
4140 steel (tempered @ 370°C)	2.4
4340 steel (tempered @ 260°C)	1.5
7075 aluminum (T651)	1.2

Equation 8.21W into Equation 8.20W, after some rearrangement, yields the following expression:

$$p = \frac{2}{Y^2 \pi r}\left(\frac{K_{Ic}^2}{\sigma_y}\right) \tag{8.22W}$$

Hence, for some given spherical vessel of radius r, the maximum allowable pressure consistent with this leak-before-break criterion is proportional to K_{Ic}^2/σ_y. The same several materials are ranked according to this ratio in Table 8.3W; as may be noted, the medium carbon steel will contain the greatest pressures.

Of the eleven metal alloys that are listed in Table B.5, the medium carbon steel ranks first according to both yielding and leak-before-break criteria. For these reasons, many pressure vessels are constructed of medium carbon steels when temperature extremes and corrosion need not be considered.

8.9W Crack Initiation and Propagation (Detailed Version)

The process of fatigue failure is characterized by three distinct steps: (1) crack initiation, wherein a small crack forms at some point of high stress concentration; (2) crack propagation, during which this crack advances incrementally with each stress cycle; and (3) final failure, which occurs very rapidly once the advancing crack has reached a critical size. The fatigue life N_f, the total number of cycles to failure, therefore can be taken as the sum of the number of cycles for crack initiation N_i and crack propagation N_p:

$$N_f = N_i + N_p \tag{8.23W}$$

The contribution of the final failure step to the total fatigue life is insignificant since it occurs so rapidly. Relative proportions to the total life of N_i and N_p depend on the particular material and test conditions. At low stress levels (i.e., for high-cycle fatigue), a large fraction of the fatigue life is utilized in crack initiation. With increasing stress level, N_i decreases and the cracks form more rapidly. Thus, for low-cycle fatigue (high stress levels), the propagation step predominates (i.e., $N_p > N_i$).

Cracks associated with fatigue failure almost always initiate (or nucleate) on the surface of a component at some point of stress concentration. Crack nucleation sites include surface scratches, sharp fillets, keyways, threads, dents, and the like. In addition, cyclic loading can produce microscopic surface discontinuities resulting from dislocation slip steps that may also act as stress raisers, and therefore as crack initiation sites.

Once a stable crack has nucleated, it then initially propagates very slowly and, in polycrystalline metals, along crystallographic planes of high shear stress; this is sometimes termed *stage I propagation* (Figure 8.10W). This stage may constitute a large or small fraction of the total fatigue life depending on stress level and the nature of the test specimen; high stresses and the presence of notches favor a short-lived stage I. In polycrystalline metals, cracks normally extend through only several grains during this propagation stage. The fatigue surface that is formed during stage I propagation has a flat and featureless appearance.

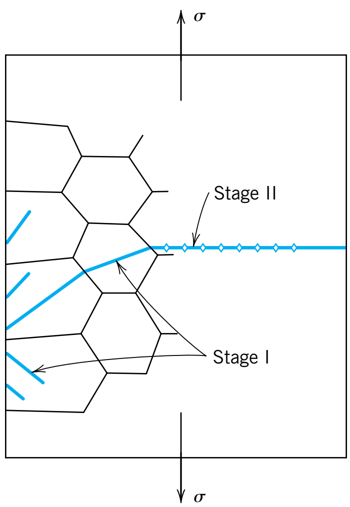

Figure 8.10W Schematic representation showing stages I and II of fatigue crack propagation in polycrystalline metals. (Copyright ASTM. Reprinted with permission.)

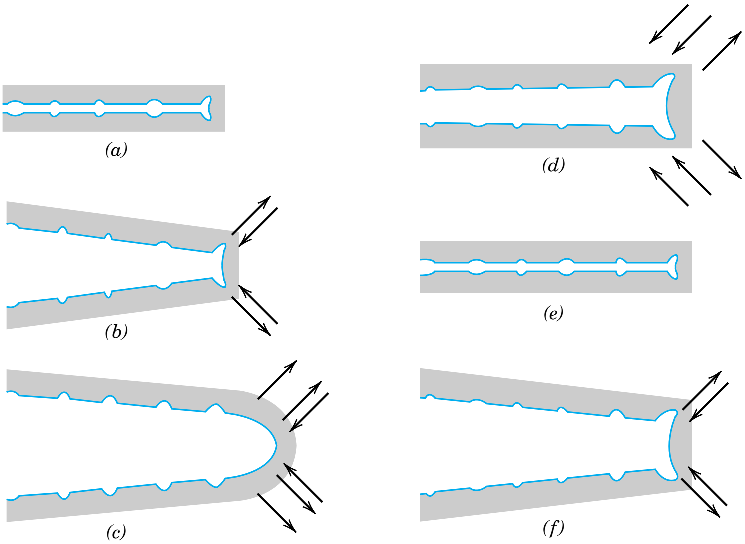

FIGURE 8.11W Fatigue crack propagation mechanism (stage II) by repetitive crack tip plastic blunting and sharpening: (*a*) zero or maximum compressive load, (*b*) small tensile load, (*c*) maximum tensile load, (*d*) small compressive load, (*e*) zero or maximum compressive load, (*f*) small tensile load. The loading axis is vertical. (Copyright ASTM. Reprinted with permission.)

Eventually, a second propagation stage (*stage II*) takes over, in which the crack extension rate increases dramatically. Furthermore, at this point there is also a change in propagation direction to one that is roughly perpendicular to the applied tensile stress (see Figure 8.10W). During this stage of propagation, crack growth proceeds by a repetitive plastic blunting and sharpening process at the crack tip, a mechanism illustrated in Figure 8.11W. At the beginning of the stress cycle (zero or maximum compressive load), the crack tip has the shape of a sharp double-notch (Figure 8.11*a*W). As the tensile stress is applied (Figure 8.11*b*W), localized deformation occurs at each of these tip notches along slip planes that are oriented at 45° angles relative to the plane of the crack. With increased crack widening, the tip advances by continued shear deformation and the assumption of a blunted configuration (Figure 8.11*c*W). During compression, the directions of shear deformation at the crack tip are reversed (Figure 8.11*d*W) until, at the culmination of the cycle, a new sharp double-notch tip has formed (Figure 8.11*e*W). Thus, the crack tip has advanced a one-notch distance during the course of a complete cycle. This process is repeated with each subsequent cycle until eventually some critical crack dimension is achieved that precipitates the final failure step and catastrophic failure ensues.

The region of a fracture surface that formed during stage II propagation may be characterized by two types of markings termed *beachmarks* and *striations*. Both of these features indicate the position of the crack tip at some point in time and appear as concentric ridges that expand away from the crack initiation site(s), frequently in a circular or semicircular pattern. Beachmarks (sometimes also called "clamshell marks") are of macroscopic dimensions (Figure 8.12W), and may be observed with the unaided eye. These markings are found for components that experienced interruptions during stage II propagation—for example, a machine that operated only during normal work-shift hours. Each beachmark band represents a period of time over which crack growth occurred.

On the other hand, fatigue striations are microscopic in size and subject to observation with the electron microscope (either TEM or SEM). Figure 8.13W is an electron fractograph that shows this feature. Each striation is thought to represent

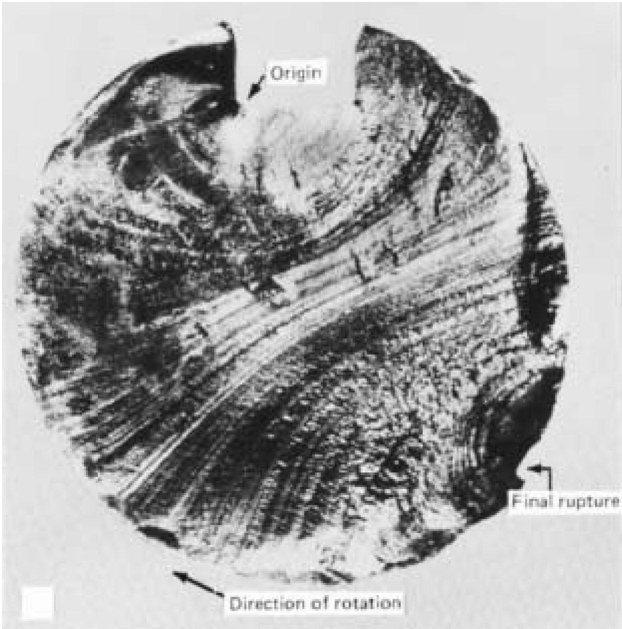

FIGURE 8.12W Fracture surface of a rotating steel shaft that experienced fatigue failure. Beachmark ridges are visible in the photograph. (Reproduced with permission from D. J. Wulpi, *Understanding How Components Fail,* American Society for Metals, Materials Park, OH, 1985.)

the advance distance of a crack front during a single load cycle. Striation width depends on, and increases with, increasing stress range.

At this point it should be emphasized that although both beachmarks and striations are fatigue fracture surface features having similar appearances, they are nevertheless different, both in origin and size. There may be literally thousands of striations within a single beachmark.

Often the cause of failure may be deduced after examination of the failure surfaces. The presence of beachmarks and/or striations on a fracture surface confirms

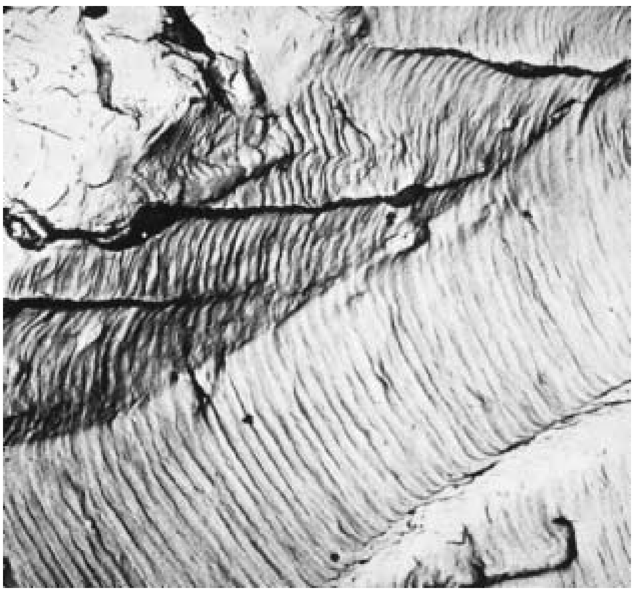

FIGURE 8.13W Transmission electron fractograph showing fatigue striations in aluminum. Magnification unknown. (From V. J. Colangelo and F. A. Heiser, *Analysis of Metallurgical Failures,* 2nd edition. Copyright © 1987 by John Wiley & Sons, New York. Reprinted by permission of John Wiley & Sons, Inc.)

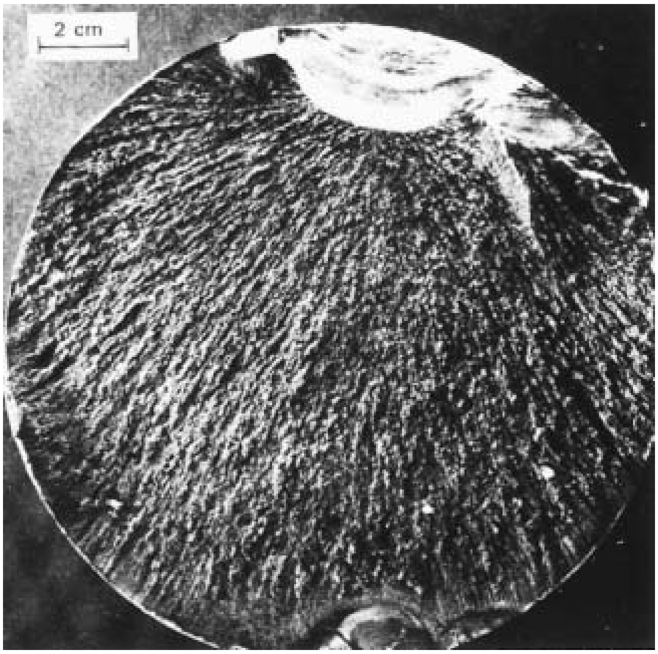

Figure 8.14W Fatigue failure surface. A crack formed at the top edge. The smooth region also near the top corresponds to the area over which the crack propagated slowly. Rapid failure occurred over the area having a dull and fibrous texture (the largest area). Approximately 0.5 ×. [Reproduced by permission from *Metals Handbook: Fractography and Atlas of Fractographs,* Vol. 9, 8th edition, H. E. Boyer (Editor), American Society for Metals, 1974.]

that the cause of failure was fatigue. Nevertheless, the absence of either or both does not exclude fatigue as the cause of failure.

One final comment regarding fatigue failure surfaces: Beachmarks and striations will not appear on that region over which the rapid failure occurs. Rather, the rapid failure may be either ductile or brittle; evidence of plastic deformation will be present for ductile failure and absent for brittle failure. This region of failure may be noted in Figure 8.14W.

8.10W Crack Propagation Rate

Even though measures may be taken to minimize the possibility of fatigue failure, cracks and crack nucleation sites will always exist in structural components. Under the influence of cyclic stresses, cracks will inevitably form and grow; this process, if unabated, can ultimately lead to failure. The intent of the present discussion is to develop a criterion whereby fatigue life may be predicted on the basis of material and stress state parameters. Principles of fracture mechanics (Section 8.5W) will be employed inasmuch as the treatment involves determination of a maximum crack length that may be tolerated without inducing failure. Note that this discussion relates to the domain of high-cycle fatigue—that is, for fatigue lives greater than about 10^4 to 10^5 cycles.

Results of fatigue studies have shown that the life of a structural component may be related to the rate of crack growth. During stage II propagation, cracks may grow from a barely perceivable size to some critical length. Experimental techniques are available that are employed to monitor crack length during the cyclic stressing. Data are recorded and then plotted as crack length a versus the number of cycles N.[6] A typical plot is shown in Figure 8.15W, where curves are included from data generated at two different stress levels; the initial crack length a_0 for both sets of tests is the same. Crack growth rate da/dN is taken as the slope at some point of the curve. Two important results are worth noting: (1) initially, growth rate is small, but increases with increasing crack length; and (2) growth rate is enhanced with increasing applied stress level and for a specific crack length (a_1 in Figure 8.15W).

Fatigue crack propagation rate during stage II is a function of not only stress level and crack size but also material variables. Mathematically, this rate may be expressed in terms of the stress intensity factor K (developed using fracture mechanics in Section 8.5W) and takes the form

$$\frac{da}{dN} = A(\Delta K)^m \tag{8.24W}$$

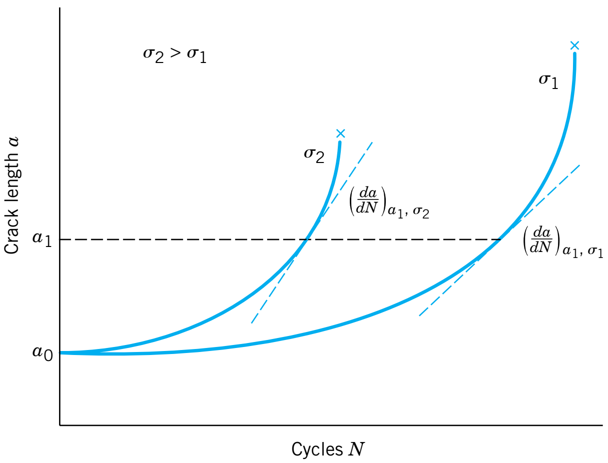

Figure 8.15W Crack length versus the number of cycles at stress levels σ_1 and σ_2 for fatigue studies. Crack growth rate da/dN is indicated at crack length a_1 for both stress levels.

[6] The symbol N in the context of Section 8.8 represents the number of cycles to fatigue failure; in the present discussion it denotes the number of cycles associated with some crack length prior to failure.

The parameters A and m are constants for the particular material, which will also depend on environment, frequency, and the stress ratio (R in Equation 8.17). The value of m normally ranges between 1 and 6.

Furthermore, ΔK is the stress intensity factor range at the crack tip; that is,

$$\Delta K = K_{\max} - K_{\min} \tag{8.25aW}$$

or, from Equation 8.10W,

$$\Delta K = Y \Delta\sigma \sqrt{\pi a} = Y(\sigma_{\max} - \sigma_{\min})\sqrt{\pi a} \tag{8.25bW}$$

Since crack growth stops or is negligible for a compression portion of the stress cycle, if $\sigma_{\min}$ is compressive, then $K_{\min}$ and $\sigma_{\min}$ are taken to be zero; that is, $\Delta K = K_{\max}$ and $\Delta\sigma = \sigma_{\max}$. Also note that $K_{\max}$ and $K_{\min}$ in Equation 8.25aW represent stress intensity factors, not the fracture toughness K_c or the plane strain fracture toughness K_{Ic}.

The typical fatigue crack growth rate behavior of materials is represented schematically in Figure 8.16W as the logarithm of crack growth rate da/dN versus the logarithm of the stress intensity factor range ΔK. The resulting curve has a sigmoidal shape that may be divided into three distinct regions, labeled I, II, and III. In region I (at low stress levels and/or small crack sizes), preexisting cracks will not grow with cyclic loading. Furthermore, associated with region III is accelerated crack growth, which occurs just prior to the rapid fracture.

The curve is essentially linear in region II, which is consistent with Equation 8.24W. This may be confirmed by taking the logarithm of both sides of this

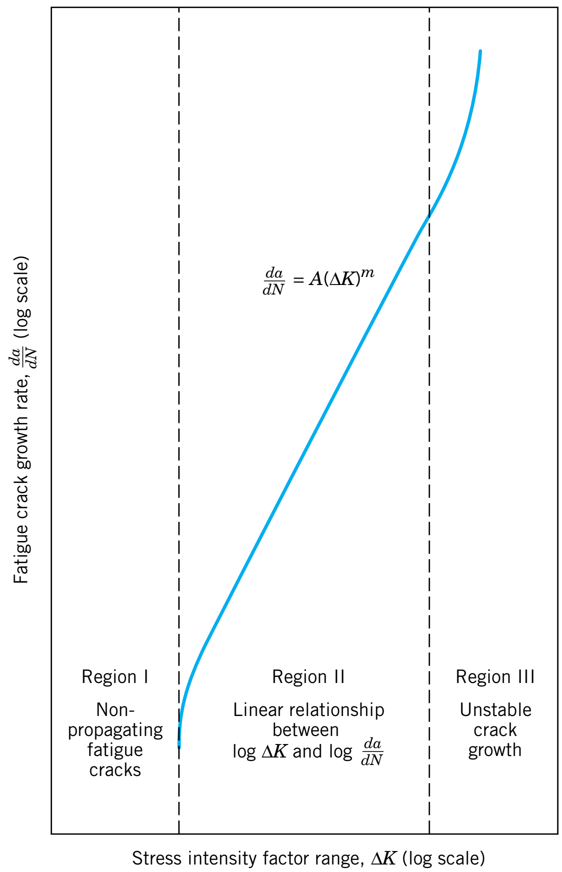

FIGURE 8.16W Schematic representation of logarithm fatigue crack propagation rate da/dN versus logarithm stress intensity factor range ΔK. The three regions of different crack growth response (I, II, and III) are indicated. (Reprinted with permission from ASM International, Metals Park, OH 44073-9989. W. G. Clark, Jr., "How Fatigue Crack Initiation and Growth Properties Affect Material Selection and Design Criteria," *Metals Engineering Quarterly*, Vol. 14, No. 3, 1974.)

expression, which leads to

$$\log\left(\frac{da}{dN}\right) = \log[A(\Delta K)^m] \tag{8.26aW}$$

$$\log\left(\frac{da}{dN}\right) = m \log \Delta K + \log A \tag{8.26bW}$$

Indeed, according to Equation 8.26bW, a straight-line segment will result when $\log(da/dN)$-versus-$\log \Delta K$ data are plotted; the slope and intercept correspond to the values of m and $\log A$, respectively, which may be determined from test data that have been represented in the manner of Figure 8.16W. Figure 8.17W is one

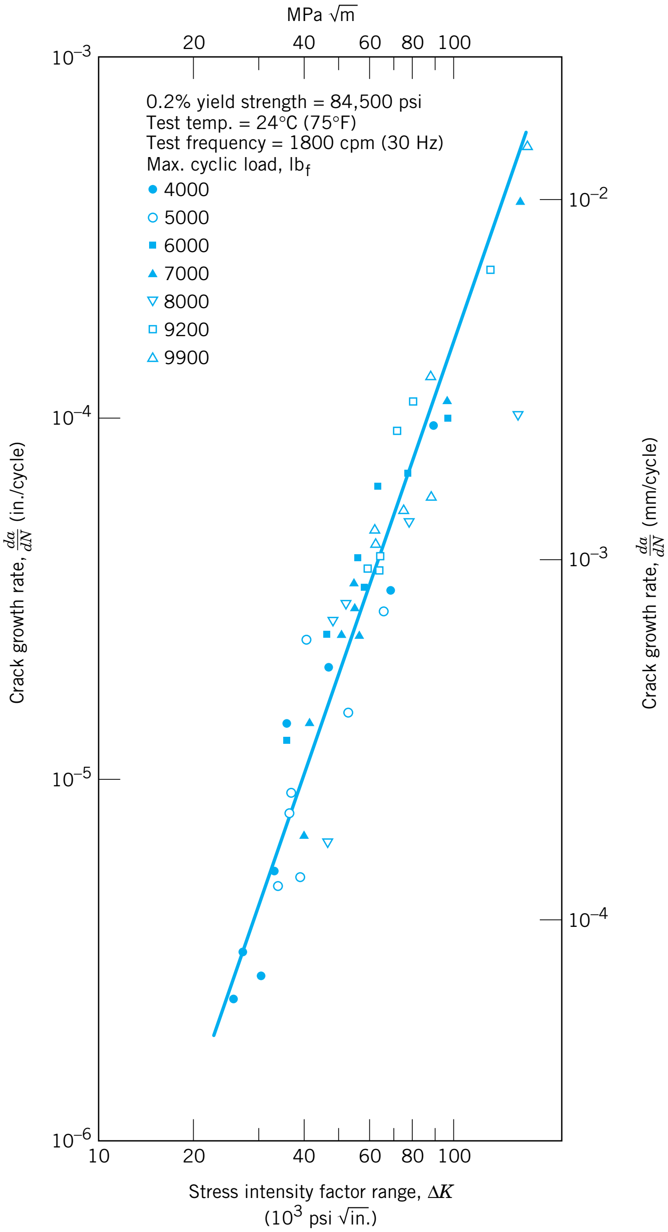

FIGURE 8.17W Logarithm crack growth rate versus logarithm stress intensity factor range for a Ni–Mo–V steel. (Reprinted by permission of the Society for Experimental Mechanics, Inc.)

such plot for a Ni–Mo–V steel alloy. The linearity of the data may be noted, which verifies the power law relationship of Equation 8.24W.

One of the goals of failure analysis is to be able to predict fatigue life for some component, given its service constraints and laboratory test data. We are now able to develop an analytical expression for N_f, due to stage II, by integration of Equation 8.24W. Rearrangement is first necessary as follows:

$$dN = \frac{da}{A(\Delta K)^m} \tag{8.27W}$$

which may be integrated as

$$N_f = \int_0^{N_f} dN = \int_{a_0}^{a_c} \frac{da}{A(\Delta K)^m} \tag{8.28W}$$

The limits on the second integral are between the initial flaw length a_0, which may be measured using nondestructive examination techniques, and the critical crack length a_c determined from fracture toughness tests.

Substitution of the expression for ΔK (Equation 8.25bW) leads to

$$\begin{aligned} N_f &= \int_{a_0}^{a_c} \frac{da}{A(Y\Delta\sigma\sqrt{\pi a})^m} \\ &= \frac{1}{A\pi^{m/2}(\Delta\sigma)^m} \int_{a_0}^{a_c} \frac{da}{Y^m a^{m/2}} \end{aligned} \tag{8.29W}$$

Here it is assumed that $\Delta\sigma$ (or $\sigma_{\max} - \sigma_{\min}$) is constant; furthermore, in general Y will depend on crack length a and therefore cannot be removed from within the integral.

A word of caution: Equation 8.29W presumes the validity of Equation 8.24W over the entire life of the component; it ignores the time taken to initiate the crack and also for final failure. Therefore, this expression should only be taken as an estimate of N_f.

Design Example 8.2W

A relatively large sheet of steel is to be exposed to cyclic tensile and compressive stresses of magnitudes 100 MPa and 50 MPa, respectively. Prior to testing, it has been determined that the length of the largest surface crack is 2.0 mm (2×10^{-3} m). Estimate the fatigue life of this sheet if its plane strain fracture toughness is 25 MPa$\sqrt{\text{m}}$ and the values of m and A in Equation 8.24W are 3.0 and 1.0×10^{-12}, respectively, for $\Delta\sigma$ in MPa and a in m. Assume that the parameter Y is independent of crack length and has a value of 1.0.

Solution

It first becomes necessary to compute the critical crack length a_c, the integration upper limit in Equation 8.29W. Equation 8.16W is employed for this computation, assuming a stress level of 100 MPa, since this is the maximum tensile stress.

Therefore,

$$a_c = \frac{1}{\pi}\left(\frac{K_{Ic}}{\sigma Y}\right)^2$$
$$= \frac{1}{\pi}\left(\frac{25 \text{ MPa}\sqrt{\text{m}}}{(100 \text{ MPa})(1)}\right)^2 = 0.02 \text{ m}$$

We now want to solve Equation 8.29W using 0.002 m as the lower integration limit a_0, as stipulated in the problem. The value of $\Delta\sigma$ is just 100 MPa, the magnitude of the tensile stress, since $\sigma_{\min}$ is compressive. Therefore, integration yields

$$N_f = \frac{1}{A\pi^{m/2}(\Delta\sigma)^m}\int_{a_0}^{a_c}\frac{da}{Y^m a^{m/2}}$$
$$= \frac{1}{A\pi^{3/2}(\Delta\sigma)^3\, Y^3}\int_{a_0}^{a_c} a^{-3/2}\, da$$
$$= \frac{1}{A\pi^{3/2}(\Delta\sigma)^3\, Y^3}(-2)a^{-1/2}\Big|_{a_0}^{a_c}$$
$$= \frac{2}{A\pi^{3/2}(\Delta\sigma)^3\, Y^3}\left(\frac{1}{\sqrt{a_0}} - \frac{1}{\sqrt{a_c}}\right)$$
$$= \frac{2}{(1.0 \times 10^{-12})(\pi)^{3/2}(100)^3(1)^3}\left(\frac{1}{\sqrt{0.002}} - \frac{1}{\sqrt{0.02}}\right)$$
$$= 5.49 \times 10^6 \text{ cycles}$$

CASE STUDY

8.13W Automobile Valve Spring

MECHANICS OF SPRING DEFORMATION

The basic function of a spring is to store mechanical energy as it is initially elastically deformed and then recoup this energy at a later time as the spring recoils. In this section helical springs that are used in mattresses and in retractable pens and as suspension springs in automobiles are discussed. A stress analysis will be conducted on this type of spring, and the results will then be applied to a valve spring that is utilized in automobile engines.

Consider the helical spring shown in Figure 8.18W, which has been constructed of wire having a circular cross section of diameter d; the coil center-to-center diameter is denoted as D. The application of a compressive force F causes a twisting force, or moment, denoted T, as shown in the figure. A combination of shear stresses result, the sum of which, τ, is

$$\tau = \frac{8FD}{\pi d^3} K_w \tag{8.30W}$$

where K_w is a force-independent constant that is a function of the D/d ratio:

$$K_w = 1.60 \left(\frac{D}{d}\right)^{-0.140} \tag{8.31W}$$

In response to the force F, the coiled spring will experience deflection, which will be assumed to be totally elastic. The amount of deflection per coil of spring, δ_c, as indicated in Figure 8.19W, is given by the expression

$$\delta_c = \frac{8FD^3}{d^4 G} \tag{8.32W}$$

where G is the shear modulus of the material from which the spring is constructed. Furthermore, δ_c may be computed from the total spring deflection, δ_s, and the

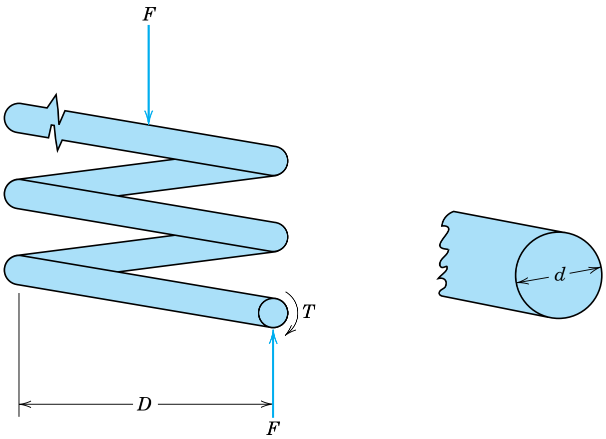

Figure 8.18W Schematic diagram of a helical spring showing the twisting moment T that results from the compressive force F. (Adapted from K. Edwards and P. McKee, *Fundamentals of Mechanical Component Design*. Copyright © 1991 by McGraw-Hill, Inc. Reproduced with permission of The McGraw-Hill Companies.)

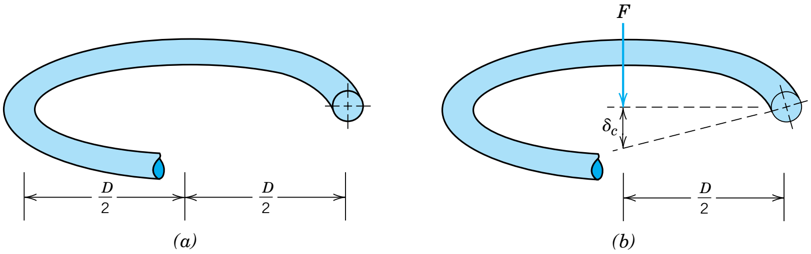

FIGURE 8.19W Schematic diagrams of one coil of a helical spring, (*a*) prior to being compressed, and (*b*) showing the deflection δ_c produced from the compressive force *F*. (Adapted from K. Edwards and P. McKee, *Fundamentals of Mechanical Component Design.* Copyright © 1991 by McGraw-Hill, Inc. Reproduced with permission of The McGraw-Hill Companies.)

number of effective spring coils, N_c, as

$$\boxed{\delta_c = \frac{\delta_s}{N_c}} \tag{8.33W}$$

Now, solving for F in Equation 8.32W gives

$$F = \frac{d^4 \delta_c G}{8D^3} \tag{8.34W}$$

and substituting for F in Equation 8.30W leads to

$$\boxed{\tau = \frac{\delta_c G d}{\pi D^2} K_w} \tag{8.35W}$$

Under normal circumstances, it is desired that a spring experience no permanent deformation upon loading; this means that the right-hand side of Equation 8.35W must be less than the shear yield strength τ_y of the spring material, or that

$$\boxed{\tau_y > \frac{\delta_c G d}{\pi D^2} K_w} \tag{8.36W}$$

AUTOMOBILE VALVE SPRING

We shall now apply the results of the preceding section to an automobile valve spring. A cutaway schematic diagram of an automobile engine showing these springs is presented in Figure 8.20W. Functionally, springs of this type permit both intake and exhaust valves to alternately open and close as the engine is in operation. Rotation of the camshaft causes a valve to open and its spring to be compressed, so that the load on the spring is increased. The stored energy in the spring then forces the valve to close as the camshaft continues its rotation. This process occurs for each valve for each engine cycle, and over the lifetime of the engine it occurs many millions of times. Furthermore, during normal engine operation, the temperature of the springs is approximately 80°C (175°F).

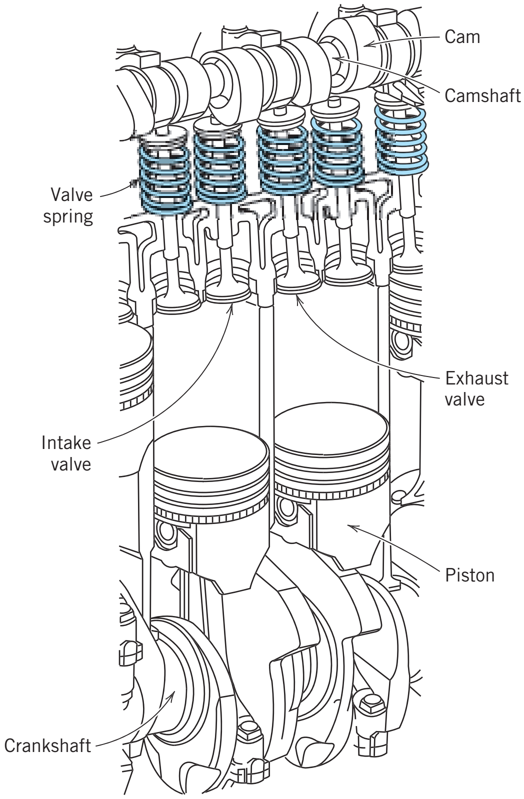

Figure 8.20W Cutaway drawing of a section of an automobile engine in which various components including valves and valve springs are shown.

A photograph of a typical valve spring is shown in Figure 8.21W. The spring has a total length of 1.67 in. (42 mm), is constructed of wire having a diameter d of 0.170 in. (4.3 mm), has six coils (only four of which are active), and has a center-to-center diameter D of 1.062 in. (27 mm). Furthermore, when installed and when a valve is completely closed, its spring is compressed a total of 0.24 in. (6.1 mm),

Figure 8.21W Photograph of a typical automobile valve spring.

which, from Equation 8.33W, gives an installed deflection per coil δ_{ic} of

$$\delta_{ic} = \frac{0.24 \text{ in.}}{4 \text{ coils}} = 0.060 \text{ in./coil } (1.5 \text{ mm/coil})$$

The cam lift is 0.30 in. (7.6 mm), which means that when the cam completely opens a valve, the spring experiences a maximum total deflection equal to the sum of the valve lift and the compressed deflection, namely, 0.30 in. + 0.24 in. = 0.54 in. (13.7 mm). Hence, the maximum deflection per coil, δ_{mc}, is

$$\delta_{mc} = \frac{0.54 \text{ in.}}{4 \text{ coils}} = 0.135 \text{ in./coil } (3.4 \text{ mm/coil})$$

Thus, we have available all of the parameters in Equation 8.36W (taking $\delta_c = \delta_{mc}$), except for τ_y, the required shear yield strength of the spring material.

However, the material parameter of interest is really not τ_y inasmuch as the spring is continually stress cycled as the valve opens and closes during engine operation; this necessitates designing against the possibility of failure by fatigue rather than against the possibility of yielding. This fatigue complication is handled by choosing a metal alloy that has a fatigue limit (Figure 8.17*a*) that is greater than the cyclic stress amplitude to which the spring will be subjected. For this reason, steel alloys, which have fatigue limits, are normally employed for valve springs.

When using steel alloys in spring design, two assumptions may be made if the stress cycle is reversed (if $\tau_m = 0$, where τ_m is the mean stress, or, equivalently, if $\tau_{\text{max}} = -\tau_{\text{min}}$, in accordance with Equation 8.14 and as noted in Figure 8.22W). The first of these assumptions is that the fatigue limit of the alloy (expressed as stress amplitude) is 45,000 psi (310 MPa), the threshold of which occurs at about 10^6 cycles. Secondly, for torsion and on the basis of experimental data, it has been found that the fatigue strength at 10^3 cycles is $0.67TS$, where TS is the tensile strength of the material (as measured from a pure tension test). The *S–N* fatigue diagram (i.e., stress amplitude versus logarithm of the number of cycles to failure) for these alloys is shown in Figure 8.23W.

Now let us estimate the number of cycles to which a typical valve spring may be subjected in order to determine whether it is permissible to operate within the fatigue limit regime of Figure 8.23W (i.e., if the number of cycles exceeds 10^6). For the sake of argument, assume that the automobile in which the spring is mounted travels a minimum of 100,000 miles (161,000 km) at an average speed of 40 mph (64.4 km/h), with an average engine speed of 3000 rpm (rev/min). The total time it takes

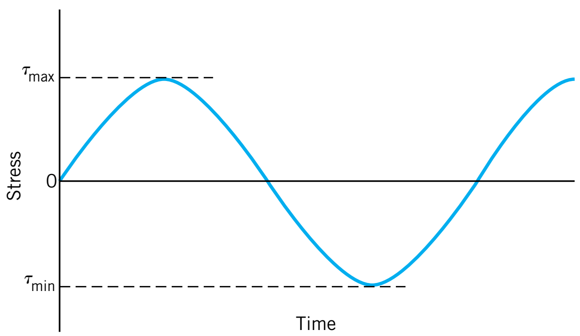

FIGURE 8.22W Stress versus time for a reversed cycle in shear.

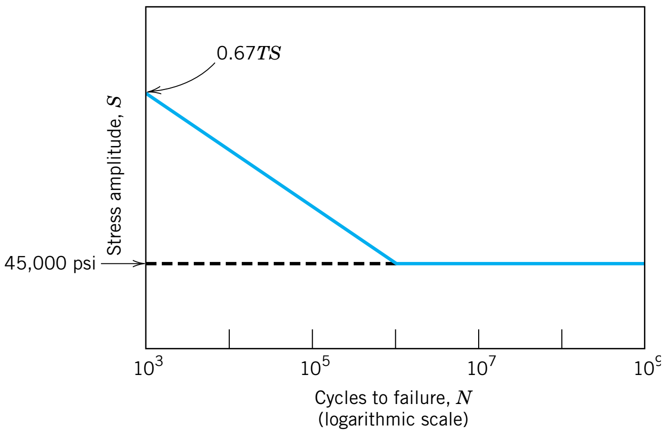

FIGURE 8.23W Shear stress amplitude versus logarithm of the number of cycles to fatigue failure for typical ferrous alloys.

the automobile to travel this distance is 2500 h (100,000 mi/40 mph), or 150,000 min. At 3000 rpm, the total number of revolutions is (3000 rev/min)(150,000 min) = 4.5 $\times$ 10^8 rev, and since there are 2 rev/cycle, the total number of cycles is 2.25 $\times$ 10^8. This result means that we may use the fatigue limit as the design stress inasmuch as the limit cycle threshold has been exceeded for the 100,000-mile distance of travel (i.e., since 2.25 $\times$ 10^8 cycles > 10^6 cycles).

Furthermore, this problem is complicated by the fact that the stress cycle is not completely reversed (i.e., $\tau_m \neq 0$) inasmuch as between minimum and maximum deflections the spring remains in compression; thus, the 45,000 psi (310 MPa) fatigue limit is not valid. What we would now like to do is first to make an appropriate extrapolation of the fatigue limit for this $\tau_m \neq 0$ case and then compute and compare with this limit the actual stress amplitude for the spring; if the stress amplitude is significantly below the extrapolated limit, then the spring design is satisfactory.

A reasonable extrapolation of the fatigue limit for this $\tau_m \neq 0$ situation may be made using the following expression (termed Goodman's law):

$$\tau_{al} = \tau_e\left(1 - \frac{\tau_m}{0.67TS}\right) \qquad (8.37\text{W})$$

where τ_{al} is the fatigue limit for the mean stress τ_m; τ_e is the fatigue limit for $\tau_m = 0$ [i.e., 45,000 psi (310 MPa)]; and, again, TS is the tensile strength of the alloy. To determine the new fatigue limit τ_{al} from the above expression necessitates the computation of both the tensile strength of the alloy and the mean stress for the spring.

One common spring alloy is an ASTM 232 chrome–vanadium steel, having a composition of 0.48–0.53 wt% C, 0.80–1.10 wt% Cr, a minimum of 0.15 wt% V, and the balance being Fe. Spring wire is normally cold drawn (Section 11.4) to the desired diameter; consequently, tensile strength will increase with the amount of drawing (i.e., with decreasing diameter). For this alloy it has been experimentally verified that, for the diameter d in inches, the tensile strength is

$$TS\text{ (psi)} = 169{,}000(d)^{-0.167} \qquad (8.38\text{W})$$

Since $d = 0.170$ in. for this spring,

$$TS = (169{,}000)(0.170 \text{ in.})^{-0.167}$$
$$= 227{,}200 \text{ psi } (1570 \text{ MPa})$$

Computation of the mean stress τ_m is made using Equation 8.14 modified to the shear stress situation as follows:

$$\tau_m = \frac{\tau_{\min} + \tau_{\max}}{2} \tag{8.39W}$$

It now becomes necessary to determine the minimum and maximum shear stresses for the spring, using Equation 8.35W. The value of $\tau_{\min}$ may be calculated from Equations 8.35W and 8.31W inasmuch as the minimum δ_c is known (i.e., $\delta_{ic} = 0.060$ in.). A shear modulus of 11.5×10^6 psi (79 GPa) will be assumed for the steel; this is the room-temperature value, which is also valid at the 80°C service temperature. Thus, $\tau_{\min}$ is just

$$\tau_{\min} = \frac{\delta_{ic} G d}{\pi D^2} K_w \tag{8.40aW}$$
$$= \frac{\delta_{ic} G d}{\pi D^2}\left[1.60\left(\frac{D}{d}\right)^{-0.140}\right]$$
$$= \left[\frac{(0.060 \text{ in.})(11.5 \times 10^6 \text{ psi})(0.170 \text{ in.})}{\pi(1.062 \text{ in.})^2}\right]\left[1.60\left(\frac{1.062 \text{ in.}}{0.170 \text{ in.}}\right)^{-0.140}\right]$$
$$= 41{,}000 \text{ psi } (280 \text{ MPa})$$

Now $\tau_{\max}$ may be determined taking $\delta_c = \delta_{mc} = 0.135$ in. as follows:

$$\tau_{\max} = \frac{\delta_{mc} G d}{\pi D^2}\left[1.60\left(\frac{D}{d}\right)^{-0.140}\right] \tag{8.40bW}$$
$$= \left[\frac{(0.135 \text{ in.})(11.5 \times 10^6 \text{ psi})(0.170 \text{ in.})}{\pi(1.062 \text{ in.})^2}\right]\left[1.60\left(\frac{1.062 \text{ in.}}{0.170 \text{ in.}}\right)^{-0.140}\right]$$
$$= 92{,}200 \text{ psi } (635 \text{ MPa})$$

Now, from Equation 8.39W,

$$\tau_m = \frac{\tau_{\min} + \tau_{\max}}{2}$$
$$= \frac{41{,}000 \text{ psi} + 92{,}200 \text{ psi}}{2} = 66{,}600 \text{ psi } (460 \text{ MPa})$$

The variation of shear stress with time for this valve spring is noted in Figure 8.24W; the time axis is not scaled, inasmuch as the time scale will depend on engine speed.

Our next objective is to determine the fatigue limit amplitude (τ_{al}) for this $\tau_m = 66{,}600$ psi (460 MPa) using Equation 8.37W and for τ_e and TS values of 45,000 psi (310 MPa) and 227,200 psi (1570 MPa), respectively. Thus,

$$\tau_{al} = \tau_e\left[1 - \frac{\tau_m}{0.67TS}\right]$$
$$= (45{,}000 \text{ psi})\left[1 - \frac{66{,}600 \text{ psi}}{(0.67)(227{,}200 \text{ psi})}\right]$$
$$= 25{,}300 \text{ psi } (175 \text{ MPa})$$

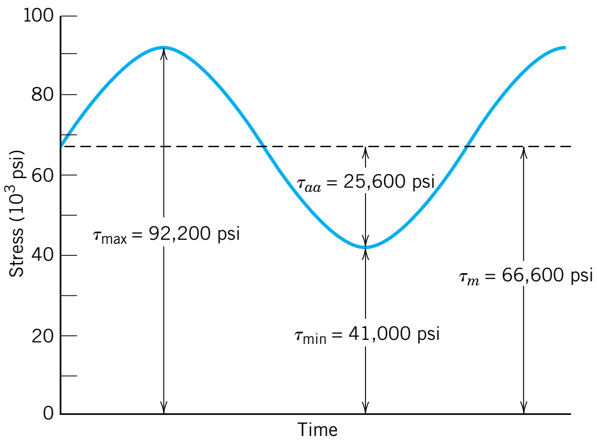

FIGURE 8.24W Shear stress versus time for an automobile valve spring.

Now let us determine the actual stress amplitude τ_{aa} for the valve spring using Equation 8.16 modified to the shear stress condition:

$$\tau_{aa} = \frac{\tau_{\max} - \tau_{\min}}{2} \tag{8.41W}$$

$$= \frac{92{,}200 \text{ psi} - 41{,}000 \text{ psi}}{2} = 25{,}600 \text{ psi (177 MPa)}$$

Thus, the actual stress amplitude is slightly greater than the fatigue limit, which means that this spring design is marginal.

The fatigue limit of this alloy may be increased to greater than 25,300 psi (175 MPa) by shot peening, a procedure described in Section 8.11. Shot peening involves the introduction of residual compressive surface stresses by plastically deforming outer surface regions; small and very hard particles are projected onto the surface at high velocities. This is an automated procedure commonly used to improve the fatigue resistance of valve springs; in fact, the spring shown in Figure 8.21W has been shot peened, which accounts for its rough surface texture. Shot peening has been observed to increase the fatigue limit of steel alloys in excess of 50% and, in addition, to reduce significantly the degree of scatter of fatigue data.

This spring design, including shot peening, may be satisfactory; however, its adequacy should be verified by experimental testing. The testing procedure is relatively complicated and, consequently, will not be discussed in detail. In essence, it involves performing a relatively large number of fatigue tests (on the order of 1000) on this shot-peened ASTM 232 steel, in shear, using a mean stress of 66,600 psi (460 MPa) and a stress amplitude of 25,600 psi (177 MPa), and for 10^6 cycles. On the basis of the number of failures, an estimate of the survival probability can be made. For the sake of argument, let us assume that this probability turns out to be 0.99999; this means that one spring in 100,000 produced will fail.

Suppose that you are employed by one of the large automobile companies that manufactures on the order of 1 million cars per year, and that the engine powering each automobile is a six-cylinder one. Since for each cylinder there are two valves, and thus two valve springs, a total of 12 million springs would be produced every year. For the above survival probability rate, the total number of spring failures would be approximately 120, which also corresponds to 120 engine failures. As a practical matter, one would have to weigh the cost of replacing these 120 engines against the cost of a spring redesign.

Redesign options would involve taking measures to reduce the shear stresses on the spring, by altering the parameters in Equations 8.31W and 8.35W. This would include either (1) increasing the coil diameter D, which would also necessitate increasing the wire diameter d, or (2) increasing the number of coils N_c.

8.16W Data Extrapolation Methods

The need often arises for engineering creep data that are impractical to collect from normal laboratory tests. This is especially true for prolonged exposures (on the order of years). One solution to this problem involves performing creep and/or creep rupture tests at temperatures in excess of those required, for shorter time periods, and at a comparable stress level, and then making a suitable extrapolation to the in-service condition. A commonly used extrapolation procedure employs the Larson–Miller parameter, defined as

$$T(C + \log t_r) \tag{8.42W}$$

where C is a constant (usually on the order of 20), for T in Kelvin and the rupture lifetime t_r in hours. The rupture lifetime of a given material measured at some specific stress level will vary with temperature such that this parameter remains constant. Or, the data may be plotted as the logarithm of stress versus the Larson–Miller parameter, as shown in Figure 8.25W. Utilization of this technique is demonstrated in the following design example.

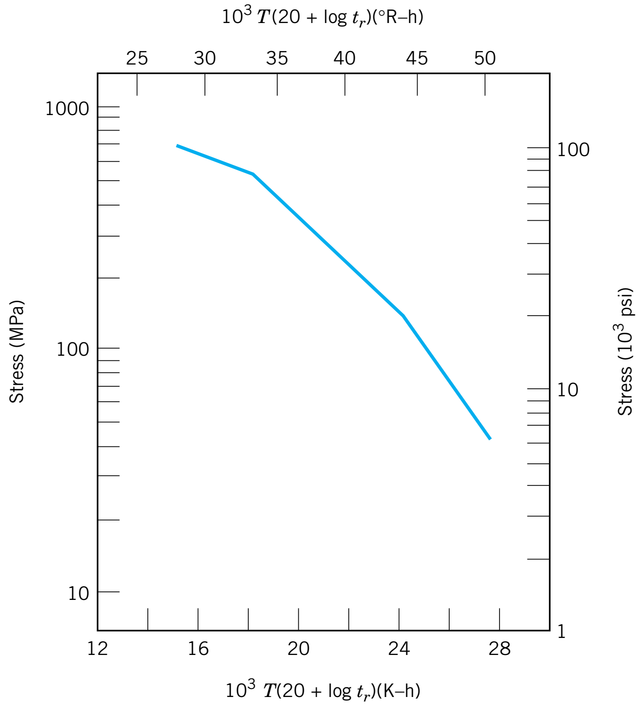

Figure 8.25W Logarithm stress versus the Larson–Miller parameter for an S-590 iron. (From F. R. Larson and J. Miller, *Trans. ASME,* **74,** 765, 1952. Reprinted by permission of ASME.)

Design Example 8.3W

Using the Larson–Miller data for S-590 iron shown in Figure 8.25W, predict the time to rupture for a component that is subjected to a stress of 140 MPa (20,000 psi) at 800°C (1073 K).

Solution

From Figure 8.25W, at 140 MPa (20,000 psi) the value of the Larson–Miller parameter is 24.0×10^3, for T in K and t_r in h; therefore,

$$\begin{aligned} 24.0 \times 10^3 &= T(20 + \log t_r) \\ &= 1073(20 + \log t_r) \end{aligned}$$

and, solving for the time,

$$\begin{aligned} 22.37 &= 20 + \log t_r \\ t_r &= 233 \text{ h } (9.7 \text{ days}) \end{aligned}$$

Chapter 9 / Phase Diagrams

9.16W The Gibbs Phase Rule

The construction of phase diagrams as well as some of the principles governing the conditions for phase equilibria are dictated by laws of thermodynamics. One of these is the **Gibbs phase rule,** proposed by the nineteenth-century physicist J. Willard Gibbs. This rule represents a criterion for the number of phases that will coexist within a system at equilibrium, and is expressed by the simple equation

$$P + F = C + N \tag{9.1W}$$

where P is the number of phases present (the phase concept is discussed in Section 9.3). The parameter F is termed the *number of degrees of freedom* or the number of externally controlled variables (e.g., temperature, pressure, composition) which must be specified to completely define the state of the system. Expressed another way, F is the number of these variables that can be changed independently without altering the number of phases that coexist at equilibrium. The parameter C in Equation 9.1W represents the number of components in the system. Components are normally elements or stable compounds and, in the case of phase diagrams, are the materials at the two extremities of the horizontal compositional axis (e.g., H_2O and $C_{12}H_{22}O_{11}$, and Cu and Ni for the phase diagrams shown in Figures 9.1 and 9.2*a*, respectively). Finally, N in Equation 9.1W is the number of noncompositional variables (e.g., temperature and pressure).

Let us demonstrate the phase rule by applying it to binary temperature–composition phase diagrams, specifically the copper–silver system, Figure 9.6. Since pressure is constant (1 atm), the parameter N is 1—temperature is the only noncompositional variable. Equation 9.1W now takes the form

$$P + F = C + 1 \tag{9.2W}$$

Furthermore, the number of components C is 2 (viz Cu and Ag), and

$$P + F = 2 + 1 = 3$$

or

$$F = 3 - P$$

Consider the case of single-phase fields on the phase diagram (e.g., α, β, and liquid regions). Since only one phase is present, $P = 1$ and

$$\begin{aligned} F &= 3 - P \\ &= 3 - 1 = 2 \end{aligned}$$

This means that to completely describe the characteristics of any alloy that exists within one of these phase fields, we must specify two parameters; these are composition and temperature, which locate, respectively, the horizontal and vertical positions of the alloy on the phase diagram.

For the situation wherein two phases coexist, for example, $\alpha + L$, $\beta + L$, and $\alpha + \beta$ phase regions, Figure 9.6, the phase rule stipulates that we have but one degree of freedom since

$$\begin{aligned} F &= 3 - P \\ &= 3 - 2 = 1 \end{aligned}$$

Thus, it is necessary to specify either temperature or the composition of one of the phases to completely define the system. For example, suppose that we decide to specify temperature for the $\alpha + L$ phase region, say, T_1 in Figure 9.1W. The compositions of the α and liquid phases (C_α and C_L) are thus dictated by the extremities of the tie line constructed at T_1 across the $\alpha + L$ field. Note that only the nature of the phases is important in this treatment and not the relative phase amounts. This is to say that the overall alloy composition could lie anywhere along this tie line constructed at temperature T_1 and still give C_α and C_L compositions for the respective α and liquid phases.

The second alternative is to stipulate the composition of one of the phases for this two-phase situation, which thereby fixes completely the state of the system. For example, if we specified C_α as the composition of the α phase that is in equilibrium with the liquid (Figure 9.1W), then both the temperature of the alloy (T_1) and the composition of the liquid phase (C_L) are established, again by the tie line drawn across the $\alpha + L$ phase field so as to give this C_α composition.

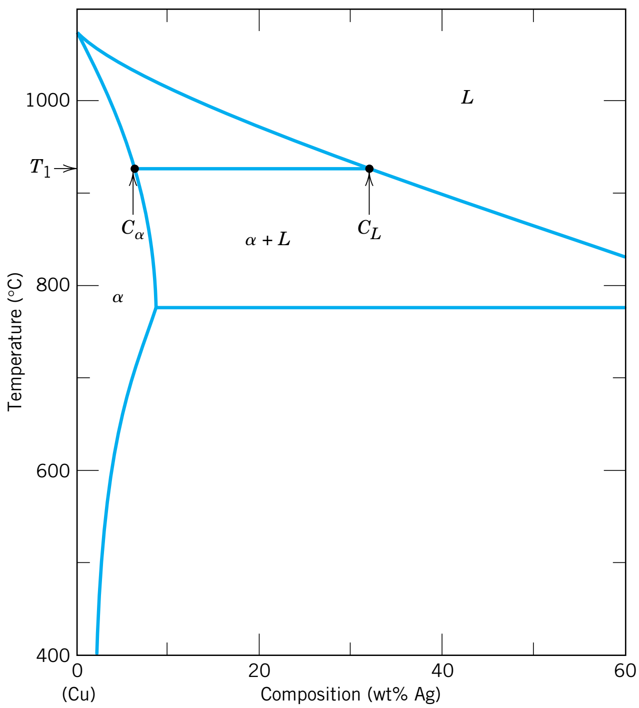

Figure 9.1W Enlarged copper-rich section of the Cu–Ag phase diagram in which the Gibbs phase rule for the coexistence of two phases (i.e., α and L) is demonstrated. Once the composition of either phase (i.e., C_α or C_L) or the temperature (i.e., T_1) is specified, values for the two remaining parameters are established by construction of the appropriate tie line.

For binary systems, when three phases are present, there are no degrees of freedom, since

$$\begin{aligned} F &= 3 - P \\ &= 3 - 3 = 0 \end{aligned}$$

This means that the compositions of all three phases as well as the temperature are fixed. This condition is met for a eutectic system by the eutectic isotherm; for the Cu–Ag system (Figure 9.6), it is the horizontal line that extends between points B and G. At this temperature, 779°C, the points at which each of the α, L, and β phase fields touch the isotherm line correspond to the respective phase compositions; namely, the composition of the α phase is fixed at 8.0 wt% Ag, that of the liquid at 71.9 wt% Ag, and that of the β phase at 91.2 wt% Ag. Thus, three-phase equilibrium will not be represented by a phase field, but rather by the unique horizontal isotherm line. Furthermore, all three phases will be in equilibrium for any alloy composition that lies along the length of the eutectic isotherm (e.g., for the Cu–Ag system at 779°C and compositions between 8.0 and 91.2 wt% Ag).

One use of the Gibbs phase rule is in analyzing for nonequilibrium conditions. For example, a microstructure for a binary alloy that developed over a range of temperatures and consisting of three phases is a nonequilibrium one; under these circumstances, three phases will exist only at a single temperature.